Journal of CO2 Utilization 83 (2024) 102792

Contents lists available at ScienceDirect

Journal of CO2 Utilization

journal homepage: www.elsevier.com/locate/jcou

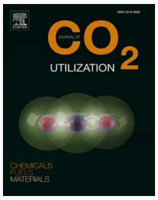

CO_2 conversion to CO by fluidized bed biomass gasification: Measuring CO_2 utilization via stable carbon isotope ratios

Florian Johann Müller [1,*], Josef Fuchs [2], Stefan Müller [3], Franz Winter [4]

Technische Universität Wien, Faculty of Technical Chemistry, Institute of Chemical, Environmental and Bioscience Engineering, Getreidemarkt 9/166, Vienna 1060, Austria

ARTICLE INFO

Keywords:
CO_2 Conversion
CCU
Gasification
Carbon
Biomass

ABSTRACT

Thermochemical conversion of CO_2 in biomass gasification is a promising technology for utilizing CO_2 as a feedstock to produce a CO-rich gas. Simultaneous decomposition reactions of biomass and various gas-solid and gas-gas reactions form the product gas in this process. The overlap in sub-processes makes it challenging to assess the conversion of feedstock CO_2 with common methods like mass balancing. This work introduces stable carbon isotope ratio analysis ($\delta^{13}C$) to identify the sourcing of carbonaceous product gas components and determine the conversion of CO_2. This methodology is applied to evaluate experiments conducted for one hour of continuous operation in a lab-scale fluidized bed gasifier. Softwood pellets and wood char are used as fuel, with Olivine as a bed material, a target heating temperature of 1000 °C and atmospheric pressure. Product gas with more than 80 vol% CO was generated when wood char was used as fuel. Stable carbon isotope measurements show that CO_2 is converted at 48–93% in this process, underpinning the position of biomass CO_2 gasification as carbon capture and utilization technology. These results were up to 25% higher than suggested by mass balancing, with higher discrepancies at lower CO_2 conversions when using softwood as fuel. Therefore, stable carbon isotope ratio measurement can be a valuable tool for improving the process understanding of biomass CO_2 gasification. The results can be used for carbon accounting and the technical development of gasifiers with high CO_2 utilization efficiency.

Nomenclature

Symbol	Parameter description	Unit
A	Cross-section of the reactor	m^2
Ar	Archimedes number	-
c_A	Volume concentration of species A in the product gas. The index $_{db,N2\text{-}free}$ describes that the volume concentration is expressed for dry-based gas(db) without nitrogen (N2-free)	%
d_P	Particle size (weighted average by sieving)	m
d_{SV}	Sauter diameter	m
f_{umf}	Factor from $\dot{V}_{mf}$ to applied feed gas flow rate	-
g	Gravity of Earth (9.81 m/s^2)	m/s^2
LHV	Lower heating value	J/Nm^3
$\dot{m}_A$	Mass flow of species or sample A	kg/s
$\dot{m}_{C\,A}$	Mass flow of carbon in species or sample A	kg/s
$^{13}R_A$	$^{13}C/^{12}C$ ratio in the species or sample A	-
RP	Reduction potential	-
T	Temperature	°C
u_{mf}	Minimum fluidization velocity	m/s
$\dot{V}_{mf}$	Minimum fluidization flow rate (normal conditions)	Nm^3/s
$\dot{V}_A$	Volume flow of species A (normal conditions)	Nm^3/s
$X_{CO2,\ stoichiometric}$	Feedstock CO_2 convertsion during gasification (calculated by product gas composition data)	%
$X_{CO2,balance}$	Feedstock CO_2 conversion during gasification (calculated by mass balance)	%

(*continued on next column*)

(*continued on next page*)

---

* Corresponding author.
E-mail addresses: florian.johann.mueller@tuwien.ac.at (F.J. Müller), josef.fuchs@tuwien.ac.at (J. Fuchs), stefan.mueller@tuwien.ac.at (S. Müller), franz.winter@tuwien.ac.at (F. Winter).

[1] https://orcid.org/0000-0002-8041-2317
[2] https://orcid.org/0000-0002-4627-4475
[3] https://orcid.org/0000-0001-8878-429X
[4] https://orcid.org/0000-0001-9854-3836

https://doi.org/10.1016/j.jcou.2024.102792
Received 27 March 2024; Received in revised form 23 April 2024; Accepted 25 April 2024

(*continued*)

Symbol	Parameter description	Unit
X_{CO2}	Feedstock CO_2 conversion during gasification (calculated by stable carbon isotope analysis)	%
$X_{CO2\ unconverted}$	Feedstock CO_2 not converted during gasification (calculated by stable carbon isotope analysis)	%
$Y_{CO\ from\ CO2}$	Share of CO in product gas derived from feedstock CO_2 (calculated by stable carbon isotope analysis)	%
$Y_{CO\ from\ fuel}$	Share of CO in product gas derived from feedstock biomass (calculated by stable carbon isotope analysis)	%
$Y_{CO2\ from\ CO2}$	Share of CO_2 in product gas derived from feedstock CO_2 (calculated by stable carbon isotope analysis)	%
$Y_{CO2\ from\ fuel}$	Share of CO_2 in product gas derived from feedstock biomass (calculated by stable carbon isotope analysis)	%
$\delta^{13}C_A$	Carbon isotope abundance in the species A compared to the VPDB standard	‰
ε_A	Isotope enrichment factor for component A (VPDB standard)	‰
μ	Dynamic viscosity (fluid)	$N*s/m^2$
ρ_F	Density (fluid)	kg/m^3
ρ_P	Density (particle)	kg/m^3
Φ	Particle sphericity	-
Abbreviation	**Term**	
CCU	Carbon Capture and Utilization	
DRI	Direct reduced ironmaking	
EA-IRMS	Elemental Analyzer - Isotope-Ratio Mass Spectrometer	
GC-C-IRMS	Gas Chromatography – Combustion - Isotope-Ratio Mass Spectrometer	
PG	Product gas	
RED III	"Renewable Energy Directive III": Directive (EU) 2023/2413 [29]	
SW	Softwood pellets	
VPDB	Vienna Peedee Belemnite	

1. Introduction

1.1. *Biomass CO_2 gasification*

Humanity's use of fossil feedstocks undoubtedly contributes significantly to global warming [1]. Carbon Capture and Utilization (CCU) technologies are promising for defossilization because CO_2 emissions from using CCU-derived products can be offset by CO_2 being captured earlier in the process, e.g., by direct air capture [2,3]. Biomass gasification with CO_2 as an oxidizer is one such CCU process [4]. The product is a carbon monoxide-rich gas, which can be combined with low-emission hydrogen as feedstock to produce commodity chemicals like acrylic acid, formic acid, methanol, or dimethyl ether [5]. Alternatively, the generated gas could be used as an energy carrier or a reducing agent in heavy industry, e.g., ironmaking via the direct reduced ironmaking (DRI) route [6].

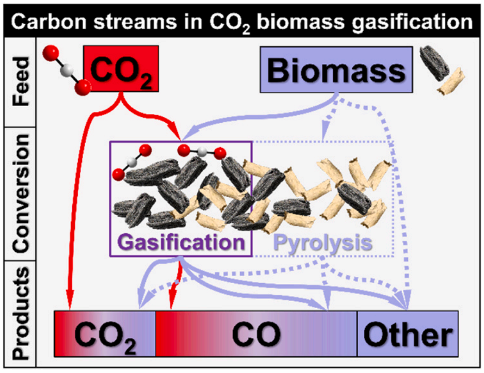

Fig. 1. Main carbon streams in biomass CO_2 gasification.

In this work, softwood, wood char, and CO_2 are denoted as parental carbon sources of carbonaceous product gas species [7]. In biomass CO_2 gasification, CO_2 is reduced in endothermic reactions while biomass undergoes drying, devolatilization or pyrolysis, and gasification processes [8,9](Table 1). These overlapping sub-processes make it challenging to differentiate between CO_2 and CO formed from the parental carbon sources CO_2 and biomass in multiple pathways (Fig. 1). This challenge results in a knowledge gap in determining how much CO_2 is utilized as a resource in this process. A new method capable of differentiating between devolatilization and CO_2 utilization is presented in this study.

Gaining further insights into the carbon streams in biomass CO_2 gasification is relevant for developing optimized biomass CO_2 gasification processes. CO_2 is mainly converted via the Boudouard-reaction (Eq. 1) [11–14], which produces CO as the primary product gas component. A high CO_2 conversion increases CO yield per biomass by using CO_2 as additional feedstock and can also improve product gas quality by lowering the CO_2 concentration in the product gas [15]. Designing a process with high CO_2 conversion based on literature is difficult because the reporting on CO_2 conversion is underdeveloped. This study provides a new way of evaluating CO_2 conversion, which should help stakeholders in this field overcome two issues with reporting in the current literature:

First, a substantial amount of literature on the topic does not investigate or discuss the role of CO_2 as a feedstock. Instead, these studies usually focus on the overall product gas composition, conversion of solid feedstock, or kinetic mechanisms and do not report CO_2 conversion results, e.g., [11,16–24]. This practice obscures how much these processes can be seen as Carbon Capture and Utilization because it remains unclear if and how much feedstock CO_2 is converted.

Table 1
Important reactions in CO_2 gasification [5,10].

Reaction	ΔH_r^0 (25 °C) in kJ/mol	Reaction name	
Heterogenous and homogenous reactions			
$C + CO_2 \leftrightarrow 2CO$	+173	Boudouard	***Eq. 1***
$C + H_2O \leftrightarrow CO + H_2$	+131	Steam-carbon (also water-gas)	***Eq. 2***
$C + 2H_2 \leftrightarrow CH_4$	-75	Methanation	***Eq. 3***
$CO + H_2O \leftrightarrow CO_2 + H_2$	-41	Water-gas shift	***Eq. 4***
Decomposition reactions of organic components			
$C_xH_yO_z \rightarrow Tar + Gas(CO, H_2, C_aH_b, CO_2) + Char(C)$	Endothermic	Pyrolysis (biomass)	***Eq. 5***
$C_xH_y \leftrightarrow (y/4)CH_4 + (x - y/4)C$	Endothermic	Pyrolysis (low O-content feedstocks)	***Eq. 6***
$C_xH_y \leftrightarrow C_{x-a}H_{y-z} + C_aH_b + ((z - b)/2)H_2$	Endothermic	Pyrolysis (low O-content feedstocks)	***Eq. 7***
$C_xH_y + xCO_2 \rightarrow 2xCO + (y/2)H_2$	Endothermic	Dry reforming	***Eq. 8***
$C_xH_y + xH_2O \rightarrow xCO + (y/2 + x)H_2$	Endothermic	Steam reforming	***Eq. 9***
$C_xH_y + (2x - y/2)H_2 \rightarrow xCH_4$	Exothermic	Hydrocracking	***Eq. 10***
$C_xH_y + CO_2 \rightarrow C_{x-1}H_{y-2} + 2CO + H_2$	Endothermic	Dry dealkylation	***Eq. 11***
$C_xH_y + H_2O \rightarrow C_{x-1}H_{y-2} + CO + 2H_2$	Endothermic	Steam dealkylation	***Eq. 12***
$C_xH_y + H_2 \rightarrow C_{x-1}H_{y-2} + CH_4$	Exothermic	Hydrodealkylation	***Eq. 13***

Table 2
Properties of fuels used in this work.

		Eucalyptus globulus Pyrolyzed wood chips [15]	**Softwood** Pelletized [40]
Proximate and ultimate analysis			
Water content	wt%	7.1	7.2
Ash content	$wt\%_{db}$	6.28	0.2
Carbon content	$wt\%_{db}$	85.42	50.7
Hydrogen content	$wt\%_{db}$	1.98	5.9
Nitrogen content	$wt\%_{db}$	0.24	0.2
Sulfur content	$wt\%_{db}$	<0.02	0.005
Chlorine content	$wt\%_{db}$	0.03	0.005
Volatile matter content	$wt\%_{db}$	15.06	85.4
Gross calorific value	kJ/kg	30,956	18,900
Net calorific value	kJ/kg	30,521	17,400
Analysis of ash melting behavior			
Deformation temperature	°C	1340	1335
Hemisphere temperature	°C	>1500	N.o.
Flow temperature	°C	>1500	1438
Ash composition			
CaO	wt%	53.0	55.2
K_2O	wt%	14.0	13.4
SiO_2	wt%	7.8	6.6
MgO	wt%	7.1	8.4
Fe_2O_3	wt%	3.8	0.9
P_2O_5	wt%	3.7	3.1
Al_2O_3	wt%	2.8	1.6
Na_2O	wt%	2.5	1.1
MnO	wt%	1.7	5.4
SO_3	wt%	1.6	2.3
Rest	wt%	2.0	1.3

*N.o… not occurred

Second, even for literature reporting on the conversion of CO_2, the results are not measured but instead are based on different calculation schemes with varying assumptions, which lowers comparability. Most calculations are based on mass balancing the investigated reactor, e.g., [25,26], but other authors instead calculate CO_2 conversion from product gas composition only [15,27]. Since rapid devolatilization processes overlap with chemical reactions (Table 1) during gasification, some assumptions must be made when assessing CO_2 conversion via mass balancing. While some authors assume all CO_2 leaving the reactor is leftover unconverted CO_2 from the CO_2 feedstock [28], other authors try to estimate the amount of CO_2 produced from the solid feedstock and subtract this from the total CO_2 in the product gas to calculate the unconverted CO_2 [25,26]. These studies further differ in the comparison case they use for this estimation. While [25] uses data from pyrolysis of the solid feedstock in a nitrogen atmosphere, [26] also proposed CO_2 formed during steam gasification for estimating CO_2 released from biomass during CO_2 gasification. For these reasons, even review papers contain little to no information on the relative conversion of CO_2 to CO in CO_2 gasification [8].

Knowing the parental carbon materials of carbonaceous gasification products is also imperative for carbon accounting. Much discussion and development of new legislation is ongoing regarding the sourcing of CO_2 for CCU processes, e.g., in the recently updated Renewable Energy Directive III (RED III). For example, RED III states that "*Emission savings from carbon capture and replacement […] shall be limited to emissions avoided through the capture of CO_2 of which carbon originates from biomass […]*" [29]. Technically, CO_2 gasification is a feedstock-flexible process not limited to sustainably sourced biomass but has historically been used to process fossil fuels, e.g., coal to synthetic Diesel [30]. CO_2 as an educt could practically also come from sources of varying sustainability: While direct air capture or biomass-based processes like bioenergy carbon capture and storage would provide CO_2 sourced from the atmosphere, other sources of CO_2 could be fossil-sourced industrial off-gases from processes like blast furnaces or coal-fired power plants. A credible measurement of carbon sources per product that does not need the addition of expensive tracer materials could be helpful for carbon accounting schemes to differentiate between carbon sources of varying sustainability.

This new study introduces stable carbon isotope analysis to attribute product gas components to their parental carbon sources by measurement. This method is proposed to enable carbon accounting and further technical improvements in CO_2 utilization for biomass CO_2 gasification or similar processes.

1.2. Stable carbon isotope analysis

Stable carbon isotope analysis has been used for decades in various scientific fields like medicine [31], biology [32], and chemistry [33]. Studies with closer relation to biomass CO_2 gasification are, e.g., kinetic studies on the CO_2-carbon reaction [34,35] or the proposal to use the differences in isotopic fingerprints of CO_2 designated for storage as markers to identify the origin of CO_2 [36]. In 2014, one study by Bhagavatula et al. used stable carbon isotope analysis to attribute product gas components to the feedstock components of biomass-coal blends in steam gasification [7]. To the authors' knowledge, no study has been published yet attributing carbonaceous product gases to CO_2 and solid feedstocks.

The stable carbon isotope ^{13}C occurs naturally with relatively small deviations, so isotope chemists usually present its concentration as a relative value compared against a standard rather than an absolute value [37]. The most widespread standard is the Vienna Peedee Belemnite (VPDB) standard [38]. It is a virtual standard replicating and replacing the previously used physical standard Peedee Belemnite based on a calcium carbonate fossil from the Peedee formation in South Carolina [38]. A value of 0.011180 or 0.0111802±0.000028 based on measurements by Chang and Li is commonly used as a $^{13}C/^{12}C$ ratio in VPDB [39]. New measurements and data are most often reported relative to this VPDB standard as isotopic abundance value $\delta^{13}C_{VPDB}$ (Eq. 14).

$$\delta^{13}C_{VPDB} = \frac{^{13}R_{sample}}{^{13}R_{VPDB}} - 1 \tag{14}$$

The $\delta^{13}C_{VPDB}$ measurements have natural abundance differences between different carbon sources. These natural abundance values of various resources are compared to values obtained in this work as part of the results (Fig. 4). CO and CO_2 in the product gas contain a mixture of carbon that entered the gasification reactor either as CO_2 or fuel (parental materials). The premise of this paper is that the different $\delta^{13}C$ values of CO_2 and biomass can be used for fingerprinting to calculate the carbon sources of CO and CO_2 by some mixing equations [7]. The mixing equations used in this work are given and discussed in Section 2.3.

2. Materials and methods

2.1. Materials

The gases air (dry, compressed), CO_2 (99.995%), and N_2 (99.999%) were supplied to the feeding line with rotameters. Water was fed by a diaphragm pump and vaporized in the hot (300 °C) feed line before entering the reactor. Two types of solid fuel were used. The first fuel was wood char chips derived from Eucalyptus globulus and prepared by pyrolysis at 700 °C for 20 minutes. These char particles' length was between 0 and approximately 15 mm. The second fuel was softwood pellets produced based on the Austrian standard ÖNORM M 7135 with a diameter of 6 mm and a mean length of about 10 mm. Ultimate analysis of both fuels was performed using an Elementar Analyzer EA 1108 CHNS-O by Carlo Erba. An Axios advanced XRF device by Panalytical Analysis gave information on the ash content based on EN ISO 18122:2015–11. Water content was determined following DIN 51718:2002–06 Method A, and volatile content following EN ISO 18123:2015–11. This information is summarized in Table 2. Wood char and softwood were selected as feedstocks because of their difference in fixed carbon and volatile content. While softwood is assumed to undergo significant devolatilization during gasification, the wood char is expected to be mainly converted by gas-solid reactions.

The fluidized bed is formed by Olivine particles, which were observed to possibly catalyze the gasification process in a previous work [15]. The Olivine used in this study contains 48–50 wt% MgO, 39–42 wt% SiO_2, and 8.0–10.5 wt% Fe_2O_3. This bed material is fluidized at lower gas flow rates than the fuel because of its smaller particle size. Feed gas velocities are selected based on fluidization calculations with the goal of fluidized Olivine particles as a bubbling bed. Appendix A and a previous work give more information on the fluidization states for the used materials and the flow rate selection [15].

2.2. Experimental setup

In continuous feeding operation, an electrically heated fluidized bed reactor with a maximum fuel input power of around 2 kW_{th} using biochar and around 3 kW_{th} using softwood pellets was used. Its schematic layout is presented in Fig. 2. This reactor is described in detail in a previous work [15]. Compared to that work, adaptations include adding a water feeding line and a sampling point for measuring stable carbon isotope ratios. Water was introduced into the gas feed line by a pump before preheating, evaporating, and heating it up to 400 °C.

The procedure described hereafter was followed to determine the $\delta^{13}C_{VPDB}$ values of feedstock and product gas samples. Gas samples were

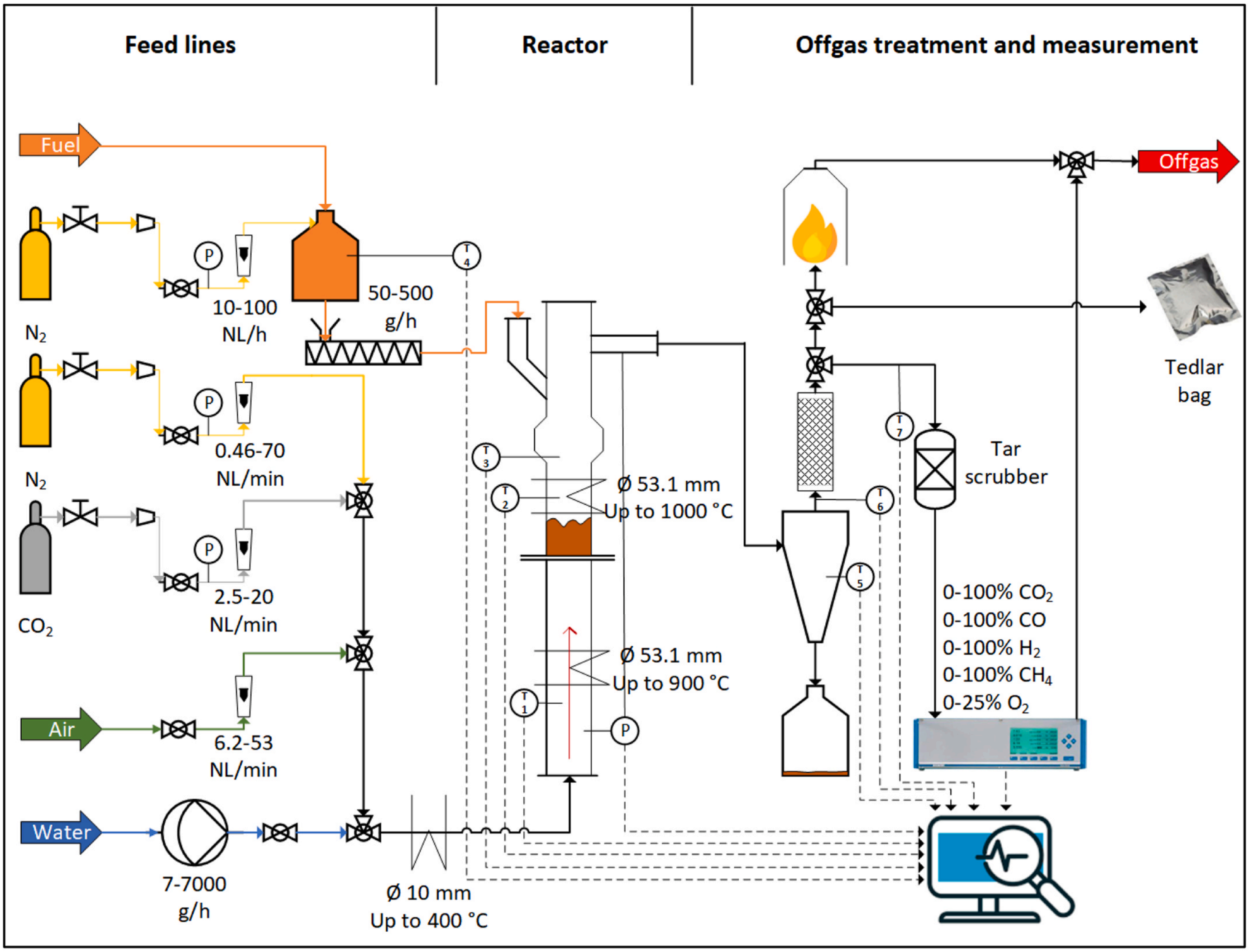

Fig. 2. Electrically heated fluidized bed reactor. Adjusted from [15].

collected in Tedlar bags during stable operation. Filling a Tedlar bag took 1–3 minutes. Therefore, the sampled gas represents an average value from such duration. A gas-tight syringe was used to prepare the gas for transport by extracting around 10 mL per sample into gas chromatography vials. For each gas sample, three vials were used to compare the results against the accepted standard deviations and average the results. These vials were sent with solid samples of softwood and char to an external laboratory to measure the relative concentration of the isotope ^{13}C in carbon monoxide and carbon dioxide. The gas samples were separated by gas chromatography, combusted, and analyzed for isotope ratio using an isotope-ratio mass spectrometer (GC-C-IRMS). The solid samples were also combusted in an elemental analyzer before entering the isotope-ratio mass spectrometer (EA-IRMS). The EA-IRMS measurement was done with a Eurovector elemental analyzer (Pavia, Italy) and a NU Horizon 1 isotope ratio mass spectrometer (Wrexham, Great Britain). The equipment used for GC-C-IRMS was: Shimadzu AOC-5000 Autosampler – Shimadzu GC2010/Shimadzu QP-2010 (Kyoto, Japan) coupled over a Hekatech combustion oven (Weinsberg, Germany) to the same NU Horizon 1 isotope ratio mass spectrometer. The measurement precision according to accreditation is ±0.63‰ for EA-IRMS and ±1.10‰ for GC-C-IRMS, given on the VPDB scale. These values include a hypothetical sampling error, which is unlikely to have happened in this work because the individual results from the triple analysis showed significantly lower standard deviations. An error estimate without this hypothetical sampling error is ±0.3‰ for EA-IRMS and ±0.5‰ for GC-C-IRMS.

2.3. Calculation

2.3.1. CO_2 conversion by stable carbon isotope analysis

This chapter describes how the CO_2 conversion X_{CO2} is calculated from stable carbon isotope ratio data ($\delta^{13}C$) and mass balancing. Balancing is performed using the process simulation software IPSEpro 8.0. IPSEpro is a steady-state, equation-oriented flowsheet simulation program. More information on the program and its use in gasification modeling is available in the literature, e.g., [41] and other publications by TUW. Appendix B has additional information on the modeling in this work.

Stable carbon isotope ratio data for the feedstocks CO_2, softwood, and wood char can be combined with the data for CO and CO_2 in product gas to calculate how much carbon of a feedstock is in which product (Eq. 15 - Eq. 18). $Y_{A\ from\ B}$ is introduced as a set of variables that describe parental carbon sourcing, or how much carbon in a product A is derived from a feedstock B. The basis of this calculation is a mixing equation, as proposed by [7]. Additionally, isotope enrichment factors ε_A are introduced in Eq. 15, Eq. 17, and Eq. 22 to account for isotopic fractionation effects. Isotopic fractionation is the change in the products' isotopic abundance that results from differences in reaction characteristics between isotopes. Differences in bond strength of ^{12}C and ^{13}C isotopes can lead to different reaction rates (kinetic isotope effect) and, therefore, to isotopic fractionation [36]. Introducing an isotope enrichment factor ε_A allows the mixing equations to account for the kinetic isotope effect and calculate the parental carbon materials' contributions to the product by removing this bias for isotopically lighter or heavier feedstocks. The sum of ε_A and the measured value $\delta^{13}C_{A,out}$ for sample A can be interpreted as the isotope ratio the experiments would theoretically have yielded for product A if no such bias existed. To the authors' knowledge, no data on isotopic enrichment factors of different product gas components in CO_2 biomass gasification are available from the literature. For this reason, two assumptions are needed to determine the isotopic fractionation factors ε_{CO} and ε_{CO2} before closing isotopic balances and calculating $Y_{A\ from\ B}$ values from measurement data.

$$Y_{CO\ from\ CO_2} = \frac{(\delta^{13}C_{CO,out} + \varepsilon_{CO}) - \delta^{13}C_{fuel}}{\delta^{13}C_{CO_2,in} - \delta^{13}C_{fuel}} \quad (15)$$

$$Y_{CO\ from\ fuel} = 1 - Y_{CO\ from\ CO_2} \quad (16)$$

$$Y_{CO_2\ from\ CO_2} = \frac{(\delta^{13}C_{CO_2,out} + \varepsilon_{CO_2}) - \delta^{13}C_{fuel}}{\delta^{13}C_{CO_2,in} - \delta^{13}C_{fuel}} \quad (17)$$

$$Y_{CO_2\ from\ fuel} = 1 - Y_{CO\ from\ CO_2} \quad (18)$$

One study tried to assess ^{13}C as a marker for CO_2 from carbon capture and storage applications [36]. It concluded that isotopic fractionation of CO_2 is likely averaging out in steam biomass gasification based on the following reason: The increased bond strength of the ^{12}C–^{13}C bond compared to ^{12}C–^{12}C suggests a ^{13}C depletion in low molecular weight gases and an enrichment in heavy components such as tar [42]. The opposite result is achieved by the water-gas shift reaction (Eq. 4), which preferably produces $^{12}CO_2$, leading to a depletion of $^{13}CO_2$ [36]. In summary, it was assumed that those effects roughly cancel each other out [36]. For this reason, the first assumption used in this work is that ε_{CO2} is negligible and can be considered zero.

A second assumption is needed to close the isotope balances and calculate ε_{CO}, because the isotope ratio in products other than CO and CO_2 was not measured in this study. This study assumes that carbon from CO_2 leaves the reactor as CO or CO_2 but not as any other carbonaceous compound, such as tar or CH_4 (Eq. 20). This assumption is based on the primary reactions in CO_2 biomass gasification, which are given in Table 1. A result of this assumption is that all carbon in species other than CO and CO_2 is derived from fuel, which means that $Y_{rest\ from\ fuel}$ in Eq. 22 has a value of 1. The subscript "rest" used for multiple variables refers to the sum of all gasification products other than CO and CO_2. The isotopic enrichment factors ε_{CO} and ε_{rest} are calculated in this study based on mass and isotope balances. Eq. 19 describes the carbon isotope balance expressed in the VPDB scale. In this balance $\dot{m}_{C,i,in}$ describes the carbon streams entering the reactor in the parental carbon materials i with the ^{13}C abundance $\delta^{13}C_{i,in}$. These input streams are balanced by the outgoing carbon streams $\dot{m}_{C,j,out}$ with the isotopic abundance $\delta^{13}C_{j,out}$, which describe all carbonaceous species leaving the reactor. The modeling of these outgoing streams also includes a stream of unconverted char, which likely was partially accumulated in the reactor during the experiments. This way of modeling ungasified char as an output stream is chosen because ungasified char is essential for closing balances, but the IPSEpro simulation is inherently steady state and does not include the option to model char accumulation dynamically. The mean isotope ratio of all carbonaceous gasification products other than CO and CO_2 ($\delta^{13}C_{rest,out}$) is calculated by Eq. 21. The variable ε_{rest} can be calculated from Eq. 22 and is briefly discussed as a plausibility check in Section 3.2.1.

A carbon exchange between CO and CO_2 during or after the gasification process could result in the products' isotopic abundance deviating from the mixture of parental carbon materials according to Eq. 15 - Eq. 19. Such an isotope equilibrium as proposed by [43], shifting isotope ratios between CO and CO_2, was investigated and ruled out in steam gasification experiments at temperatures similar to or even slightly higher than in this work [7]. The short residence time of the gas in the hot reactor also supports that such an equilibrium exchange did not significantly influence the stable carbon isotope ratio. Therefore, such an exchange is not considered in this study.

$$\sum \dot{m}_{C,i,in} \cdot \delta^{13}C_{i,in} = \sum \dot{m}_{C,j,out} \cdot \delta^{13}C_{j,out} \quad (19)$$

$$\dot{m}_{C,rest,out} = \dot{m}_{C,fuel,in} - \dot{m}_{C,CO,out} \cdot Y_{CO\ from\ fuel} - \dot{m}_{C,CO_2,out} \cdot Y_{CO_2\ from\ fuel} \quad (20)$$

$$\delta^{13}C_{rest,out} = \frac{\sum(\dot{m}_{C,i,in} \cdot \delta^{13}C_{i,in}) - \dot{m}_{C,CO_2,out} \cdot \delta^{13}C_{CO_2,out} - \dot{m}_{C,CO,out} \cdot \delta^{13}C_{CO,out}}{\dot{m}_{C,rest,out}} \quad (21)$$

Table 3
Experimental parameters investigated within this work. SW=softwood pellets. Char=pyrolyzed wood chips derived from Eucalyptus globulus.

Exp.	Heating temp. °C	Olivine height cm	CO_2 flow rate NL/min	Steam flow rate NL/min	Fuel type	Fuel feed g/min	Carbon ratio C_{fuel}:C_{CO2} mol/mol
#1	1000	10	2.8	0	SW	4.2	1.35
#2				0.23	SW	4.2	1.35
#3				0	SW	6.4	2
#4				0.23	SW	6.4	2
#5				0	Char	1.9	1
#6				0	Char	3.7	2
#7				0.36	Char	3.7	2

$$Y_{\text{rest from fuel}} = 1 = \frac{\left(\delta^{13}C_{\text{rest,out}} + \varepsilon_{\text{rest}}\right) - \delta^{13}C_{CO_2,\text{in}}}{\delta^{13}C_{\text{fuel}} - \delta^{13}C_{CO_2,\text{in}}} \tag{22}$$

Mass flow data are necessary to relate the relative parameter $Y_{CO2\ from\ CO2}$ to the flow of CO_2 going into the reactor ($\dot{m}_{CO2,in}$) and determine X_{CO2}, the conversion of CO_2 (Eq. 23 - Eq. 24). The outgoing mass flow of CO_2 ($\dot{m}_{CO2,out}$) is derived from mass balancing in IPSEpro.

$$X_{\text{CO2 unconverted}} = \frac{\dot{m}_{\text{CO2,out}}}{\dot{m}_{\text{CO2,in}}} \cdot Y_{\text{CO2 from CO2}} \tag{23}$$

$$X_{\text{CO2}} = 1 - X_{\text{CO2 unconverted}} \tag{24}$$

2.3.2. CO_2 conversion by other methods

Two calculation methods used in previous works are applied for comparison to demonstrate the variance in reported CO_2 conversion caused by different calculation methods (Eq. 25 - Eq. 26). The first calculation was proposed by [44] and uses the dry-based volumetric product gas concentrations of CO, CO_2 and H_2 (c_A). This calculation assumes all CO and H_2 in the product gas are produced by the Boudouard reaction (Eq. 1) or steam-carbon reaction (Eq. 2). It is denominated with the term *stoichiometric* in this work to differentiate between this calculation and the calculation by stable carbon isotope analysis.

$$X_{\text{CO2,stoichiometric}} = \frac{c_{CO} - c_{H2}}{c_{CO} - c_{H2} + 2 \cdot c_{CO2}} \tag{25}$$

This equation allows the calculation of $X_{CO2,stoichiometric}$ with the same time interval as available product gas composition data. The quick and continuous availability of data without mass balancing is a clear advantage of this method. However, this calculation also has some limitations [15]. An essential assumption this equation makes is the following:

- CO or H_2 are products of the Boudouard and steam carbon reactions. This assumption is most valid for feedstocks like char and coal, which have relatively limited volatile content and do not contribute significantly to the gas composition via devolatilization. With increasing volatile content, the uncertainty of the calculation can increase.

The volatile content of around 85 wt% for softwood challenges the applicability of this equation. For this reason, more significant differences between this simplified calculation and the calculation by isotopic tracing are expected when softwood as fuel is compared to wood char.

The second calculation performed for comparison is based on a mass balance of input and output streams in IPSEpro (Eq. 26). Following the calculation by [28], all CO_2 in the product gas is assumed as leftover feedstock CO_2.

$$X_{\text{CO2,balance}} = \frac{\dot{m}_{\text{CO2,in}} - \dot{m}_{\text{CO2,out}}}{\dot{m}_{\text{CO2,in}}} \tag{26}$$

2.3.3. Reduction potential

The reduction potential *RP* is introduced as a measure of product gas quality. This parameter describes the ratio of the reduced gases CO and H_2 to the fully oxidized compounds CO_2 and H_2O. This parameter is used in direct reduced ironmaking as a descriptor of the gases' ability to reduce iron ore [6]. *RP* is calculated by Eq. 27, using c_A, which is the volume concentration of species A in the product gas.

$$RP = \frac{c_{CO} + c_{H2}}{c_{CO2} + c_{H2O}} \tag{27}$$

2.4. Conducted experiments

Previous works suggest high temperature, high gas-fuel contact times, and Olivine as bed material to achieve high CO_2 conversion [15]. Accordingly, the reactor's heating was set to the maximum temperature of 1000 °C, a filling of 10 cm Olivine in the reactor was used as bed material, and a low CO_2 flow rate was adopted while still forming a bubbling fluidized bed. The fuel height in the reactor is not available as a measurement from this experimental setup in continuous operation. Instead, different ratios of carbon fed in fuel and CO_2 were used with the expectation that proportionally higher fuel feeding would also lead to a larger fuel reservoir in the reactor, thus increasing fuel-gas contact time. The Boudouard reaction demands a carbon ratio of 1 between solid carbon in fuel and CO_2. The applied carbon ratios reach or exceed this stoichiometric ratio. Experiments were conducted with softwood pellets and biochar to investigate the influence of volatile content. Higher volatile content at similar total carbon ratios could lower the CO_2 conversion because less fixed carbon is available for the Boudouard reaction after pyrolytic decomposition reactions. Some experiments were conducted with moisture in CO_2 to compare a dry CO_2 stream to a typical moist stream from a capture unit like an amine scrubber. The parameters chosen for the experiments are summarized in Table 3.

3. Results and discussion

3.1. Product gas

3.1.1. Experimental data

Experiments were continued with continuous feeding for at least one hour. All values in Section 3.1 are averaged data from one hour of operation during which the measured product gas concentration remained largely stable. Supporting information on the experimental data and their interpretation is given in Appendix C. Dry-based product gas concentrations were combined with the water content data estimated by mass balancing to calculate the product gas composition for all conducted experiments, which is shown in Fig. 3. Fig. 3 also has data on the equilibrium product gas composition at the measured reaction zone temperature calculated by the minimization of free Gibbs energy in FactSage's equilibrium module. For most experiments, the experimental data show more CO_2, H_2O and CH_4, and less CO and H_2 than the equilibrium composition. The differences between thermodynamic equilibrium and observed concentrations are more significant for softwood experiments and experiment #5 with a lower char feeding rate than #6 and #7. Experimentally determined gas compositions for experiments #6 and #7 have high CO and low CO_2 content and are very similar to the calculated equilibrium gas composition, which suggests a high

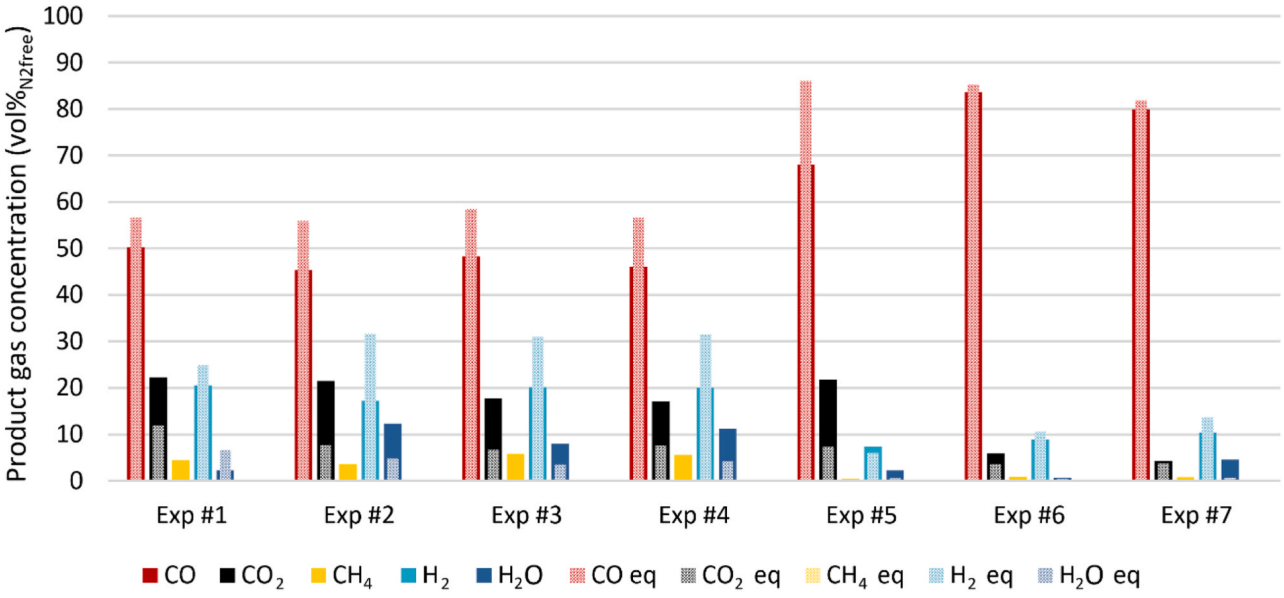

Fig. 3. Product gas composition: Measured concentrations (full bars) vs. thermodynamic equilibrium concentrations calculated in FactSage (checkered bars). H_2O concentration was not measured but is a result of mass balancing.

Table 4
Key differences in operational parameters and performance indicators for all experiments. SW=softwood pellets. Char=pyrolyzed wood chips derived from Eucalyptus globulus.

Parameter	Unit	Data source	Exp. #1	Exp. #2	Exp. #3	Exp. #4	Exp. #5	Exp. #6	Exp. #7
Fuel type	-	Setting	SW	SW	SW	SW	Char	Char	Char
Carbon ratio C_{fuel}:C_{CO2}	-	Setting	1.35	1.35	2	2	1	2	2
H_2O added	-	Setting	No	Yes	No	Yes	No	No	Yes
Temperature	°C	Measurement	903	856	821	825	877	864	856
Unconverted fuel carbon	%	Mass balance	2	12	13	14	23	46	42
$\dot{V}_{total,out}$	NL/min	Mass balance	8.6	8.5	10.6	10.7	5.4	6.3	7.0
$\dot{V}_{CO,out}$	NL/min	Mass balance	4.2	3.9	5.0	5.0	3.9	5.3	5.6
$\dot{V}_{CO2,out}$	NL/min	Mass balance	1.8	1.8	1.9	1.8	1.0	0.4	0.3
$\dot{V}_{H2,out}$	NL/min	Mass balance	1.7	1.5	2.2	2.1	0.4	0.6	0.7
$\dot{V}_{CH4,out}$	NL/min	Mass balance	0.4	0.3	0.6	0.6	0.0	0.1	0.1
$\dot{V}_{H2O,out}$	NL/min	Mass balance	0.5	1.1	0.9	1.2	0.1	0.0	0.3
H_2/CO ratio	-	Measurement	0.4	0.4	0.4	0.4	0.1	0.1	0.1
RP	-	Mass balance	2.5	1.8	2.7	2.3	3.9	14.1	10.2
$RP_{equilibrium}$	-	Gibbs energy minimization	4.4	7.1	8.8	7.5	11.6	23.2	21.3
LHV	MJ/Nm^3	Mass balance	9.8	8.8	10.3	10.0	10.0	11.8	11.5

conversion of the feedstock CO_2.

Table 4 summarizes additional data measured or calculated by mass and energy balancing in IPSEpro for all experiments. Temperatures in Table 4 are taken from temperature measurement T2 (see Fig. 2), which is positioned in the reaction zone’s center.

3.1.2. Influence of fuel type

The product gas derived from the experiments with char is very rich in carbon monoxide, dry, and comparatively lean in hydrogen. These results fit well with the data from earlier works in semi-continuous operation, which had up to 83% CO content in the produced gas when high amounts of wood char were in this reactor [15]. In experiments with softwood as fuel, the main gas component, carbon monoxide, is produced at a similar rate, but water, hydrogen, and carbon dioxide have all increased. Softwood experiments also yield some methane in the resulting product gas, which is almost absent in the experiments with char.

The larger share of H_2, H_2O, and CH_4 for experiments with softwood as fuel is caused by a higher hydrogen-to-carbon ratio in the fuel composition (Table 2). As a result, the H_2-to-CO ratio is also higher in product gas from softwood experiments. For all experiments, the H_2-to-CO ratio is too low for direct conversion of the gas to methanol or in Fischer-Tropsch-synthesis, which need an H_2-to-CO ratio of around 2:1 [3,45]. For such applications, the gas would need H_2 enrichment, e.g., by adding hydrogen from water electrolysis. In existing DRI plants, the reduction potential *RP* for the reducing gas usually has a value of around 9 or higher [6]. The gas produced in experiments #6 and #7 with char as fuel has sufficient reduction potential to fulfill this requirement without adjusting the gas composition by carbon capture or water condensation. Reduction potentials are lower when less char is fed (#5) and for all experiments conducted with softwood. The highest reduction potentials calculated for equilibrium gas compositions are achieved for experiments with high fuel feeding rate and dry CO_2 feed. For softwood experiment #3 this maximum is 8.8; for wood char experiment #6 it is 23.2.

The changes in gas composition are minor when comparing experiments with dry and wet CO_2 feed. A consistent trend is that steam flow rates in product gas increase when an H_2O/CO_2 mixture is adopted as feedstock. This increase has a detrimental effect on the reduction power and lower heating value.

Since the methanation reaction (Eq. 3) proceeds at a very slow rate at these temperatures except at high pressures [7], the observed methane for experiments with softwood is likely released by rapid pyrolysis, which proceeds the gasification of char in gasification [8,9]. The absence of CH_4 in the calculated thermodynamic equilibrium compositions further confirms that it is a decomposition product rather than a product formed via the methanation reaction. H_2, CO, and CO_2 are other typical pyrolysis products from woody biomass, typically released during gasification at equal or higher amounts than methane [46]. The increased production of devolatilization products from softwood is apparent from proximate analysis and evident when comparing the total product gas flow rates and unconverted fuel carbon values. The Boudouard reaction demands a stoichiometric parental ratio of 1:1 (Eq. 1). In experiments #6 and #7, feeding wood char with low volatile content at a carbon ratio of 2:1, the mass balance suggests that nearly half of the fuel carbon was not converted in the process. On the contrary, the unconverted solid carbon was much lower in experiments #3 and #4, which supplied the same 2:1 parental carbon ratio via softwood. This difference is explained by considering that a sizeable amount of carbon from softwood was converted to gas by decomposition reactions. The increase in devolatilization in softwood experiments results in higher total syngas flow rates. At the same time, these overlapping processes make it harder to identify the CO_2 conversion by other methods than the proposed stable carbon isotope measurement scheme.

3.1.3. *Influence of fuel feeding rate*

Increased fuel feeding was selected to achieve a larger fuel bed and increase the fuel-gas contact time, which was expected to increase CO_2 conversion based on previous findings [15]. For softwood experiments, the changes in gas composition between experiments #1 and #2 with less fuel versus #3 and #4 with more fuel are relatively small. In these experiments, the volume flows per component increase for all product gas components other than CO_2, which remains stable. This trend is similar in wood char experiments, where the outgoing CO_2 volume flow decreases at a higher fuel feeding rate. These changes in gas composition have little effect on the H_2-to-CO ratio. The reduction potential is slightly increased for softwood experiments at higher fuel feeding rates. For wood char experiments, where the volume flow rate of CO_2 in product gas decreases with higher fuel feeding rate, the reduction potential more than doubles when increasing the parental carbon ratio from 1:1–2:1. A drawback of this increase is calculated in the form of increased amounts of excess solid carbon.

Feeding softwood at a carbon ratio above 2 could increase the gases' reduction potential because too little fixed carbon might be available for the Boudouard reaction after devolatilization. However, this option is not feasible with the reactor used in this work because of limited heating capabilities. Temperatures on the reactor's outside wall are limited to 1000 °C for safety reasons. As a result, temperatures in the reaction zone are a complex result of heat transfer effects and energy demands of chemical reactions. The temperature differences for softwood experiments at carbon ratios of 1:1 versus experiments with a ratio of 2:1 in this work are likely a reason of increased energy demand for chemical reaction when a ratio of 2:1 was used. Increasing the carbon ratio even higher increases the energy demand from chemical reactions, possibly further lowering the temperature in the reaction zone. Since higher temperatures are beneficial for CO_2 conversion [15], this change might be detrimental to the reduction potential of the product gas. A dedicated experimental campaign using various gas and solid feed rates could clarify the optimum feed ratio for product gases with high reduction potential.

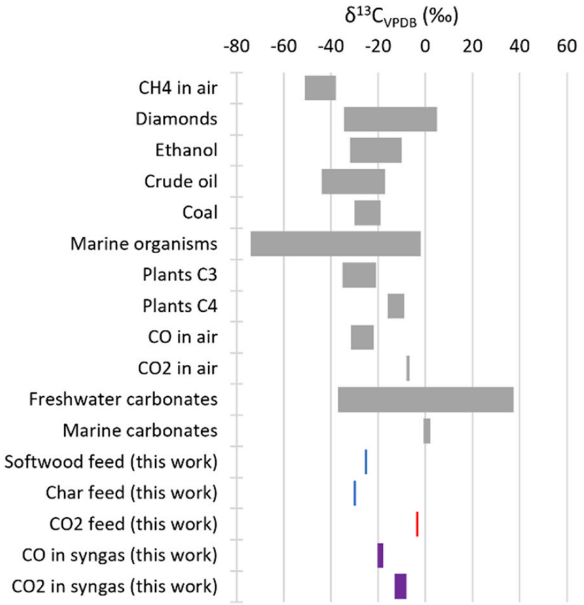

Fig. 4. Abundance of ^{13}C given as $\delta^{13}C_{VPDB}$ for various natural sources following [47] and all feeds and products in this work.

3.2. *Carbon stream analysis*

The isotope ratios measured for carbonaceous feedstocks and product gas components are given in Table 5. Some of these data are depicted in Fig. 4 and compared to natural abundance values of various carbon sources. The label "Plants C3", showing $\delta^{13}C$ values between −23 and −34‰ [36,47], describes almost 95% of plants on earth fixing carbon dioxide by the Calvin cycle [7]. Both biomass-derived feedstocks are in this stable isotope ratio range. The differences in stable carbon isotope ratio between softwood and char compared to the feedstock CO_2 are 21.8 and 26.4‰. These differences are multiple times the accredited standard deviation of ≤0.63‰ for bulk and ≤1.10‰ for gas measurements. Therefore, the differences in the natural abundance of ^{13}C in feedstock CO_2 and fuel are significant enough to differentiate between parental carbon sources. The same is true for $\delta^{13}C$ values for CO and CO_2 in the product gas, which are between the values measured for the parental carbon sources but still differ significantly from them.

3.2.1. *Isotopic fractionation*

The $\delta^{13}C$ data from measurements are expanded in Table 5 by information on the calculated isotope enrichment factors for carbon monoxide (ε_{CO}) and carbonaceous products other than CO or CO_2 (ε_{rest}). Additionally, the average stable carbon isotope ratio in products other than CO or CO_2 is calculated by isotope mass balances. More

Table 5
Stable carbon isotope ratios $\delta^{13}C$ for carbonaceous feedstocks and products in this work. PG = product gas.

	CO_2 feed $\delta^{13}C_{CO2,in}$ ‰ Measured	**Bulk feed** $\delta^{13}C_{fuel}$ ‰ Measured	**CO_2 in PG** $\delta^{13}C_{CO2,out}$ ‰ Measured	**CO in PG** $\delta^{13}C_{CO,out}$ ‰ Measured	**Enrichment factor (CO)** ε_{CO} ‰ Calculated	**Other products** $\delta^{13}C_{rest,out}$ ‰ Calculated	**Enrichment factor (rest)** ε_{rest} ‰ Calculated
Exp. #1	-3.4	-25.2	-8.0	-18.7	0.5	-21.6	-3.6
Exp. #2	-3.4	-25.2	-8.4	-19.3	1.9	-16.8	-8.4
Exp. #3	-3.4	-25.2	-11.0	-20.2	1.8	-19.0	-6.2
Exp. #4	-3.4	-25.2	-10.3	-19.7	1.2	-21.4	-3.8
Exp. #5	-3.4	-30.0	-7.8	-17.8	1.3	-23.0	-7.0
Exp. #6	-3.4	-30.0	-13.1	-18.6	1.5	-27.2	-2.8
Exp. #7	-3.4	-30.0	-11.4	-19.2	1.5	-26.6	-3.4

information on mass balancing is available in Appendix B.

The $\delta^{13}C_{rest,out}$ data summarize the average ^{13}C abundance in any carbonaceous product species other than CO and CO_2. This summary includes CH_4, higher hydrocarbons, tar, and ungasified char, of which the latter either leaves the reactor as fly char or is accumulated in the reactor during operation. The calculated values are closer to the isotope ratio of the solid parental carbon materials softwood and wood char than CO_2. The value's proximity to the fuel value is explained by ungasified char being calculated as the prevalent compound in this mix.

The resulting ε_{rest} values show some ^{13}C enrichment for this group of compounds. Since various carbon side streams are summarized in the variables $\delta^{13}C_{rest,out}$ and ε_{rest}, the exact reason for this enrichment is challenging to pin down. The literature suggests that carbon from CO_2 could be substituted into the surface of ungasified char [34], potentially enriching it in ^{13}C because the feedstock CO_2 is isotopically heavier than the used biomass. However, because of the continuous nature of the experiment in this work, such an effect seems unlikely because the fuel is continuously replaced. Another explanation can be found in the increased bond strength of the ^{12}C–^{13}C bond compared to ^{12}C–^{12}C. This bond strength difference suggests a ^{13}C depletion in low molecular weight gases and an enrichment in heavy components such as tar [42]. This explanation would also explain the positive values for the isotopic enrichment factor for CO (ε_{CO}), calculated at 0.5–1.9‰. These values mean CO was produced with a slight preference for ^{12}C during gasification. Therefore, the measured $\delta^{13}C_{CO,out}$ values are lower than they would be if no isotopic fractionation happened. The literature reports ^{13}CO enrichment after the water-gas shift reaction (Eq. 4) [36]. However, the experiments in this work were performed above 800 °C, where the reverse water-gas shift reaction becomes increasingly dominant over the water-gas shift reaction [26]. For this reason, the ^{13}CO depletion could be explained by the reverse water-gas shift reaction, introducing the reverse trend to the trend reported in the literature for the water-gas shift reaction.

The trends calculated for isotopic fractionation can be reasonably explained based on the available literature. For this reason, the two main assumptions chosen for closing the balances and described in Section 2.3 are deemed acceptable:

- feedstock CO_2 is only converted to CO in this process, and
- negligible isotopic fractionation for CO_2 occurred.

3.2.2. Parental carbon sources of CO in product gas

The stable carbon isotope ratio data given in Table 5 are used to calculate how much carbon from the parental carbon sources CO_2, softwood, and wood char is in the product gas components CO and CO_2 (Eq 15 - Eq 18). These relative contributions are combined with the volume flow data for CO and CO_2 (Table 4) to calculate CO and CO_2 volume flows in product gas per parental carbon source. Both relative and absolute data are depicted in Fig. 5. Error ranges are calculated based on the precision of EA-IRMS and GC-C-IRMS measurements without the hypothetical sampling error.

The volume flow of CO in product gas is increased when more fuel is fed (exp. #3, #4, #6, and #7). CO with carbon from CO_2 and from fuel is increased in these experiments (blue bars in Fig. 5). When more fuel is fed, CO with carbon from fuel is increased because more CO is released from pyrolysis. The increase of CO with carbon from CO_2 at higher fuel feeding rates means that more CO_2 was converted in these experiments (see Section 3.2.4). Previous works showed that an increase in fuel-gas contact time leads to higher CO_2 conversion [15]. The most important reaction for converting CO_2 in this system is the Boudouard reaction, which uses carbon from both parental sources to produce CO with an even split between both carbon sources.

The CO production from pyrolysis is more pronounced for softwood as fuel because the volatile content in wood char is low. $Y_{CO\ from\ CO2}$ is around a third when softwood is used as fuel. This number is significantly higher at around 50% when using char. While the data show that feeding more fuel allows for the conversion of more CO_2 for both softwood and wood char as fuel, $Y_{CO\ from\ CO2}$ slightly declines at higher fuel feeding rates. The reason for this is likely that increasing the fuel feeding rate increases the production of CO via pyrolysis of fuel faster than via the Boudouard reaction from CO_2. These differences observed for the experiment pairings #1|3, #2|4, and #5|6 in this study are minor at 1–5% and more experiments are necessary to confirm that the relative

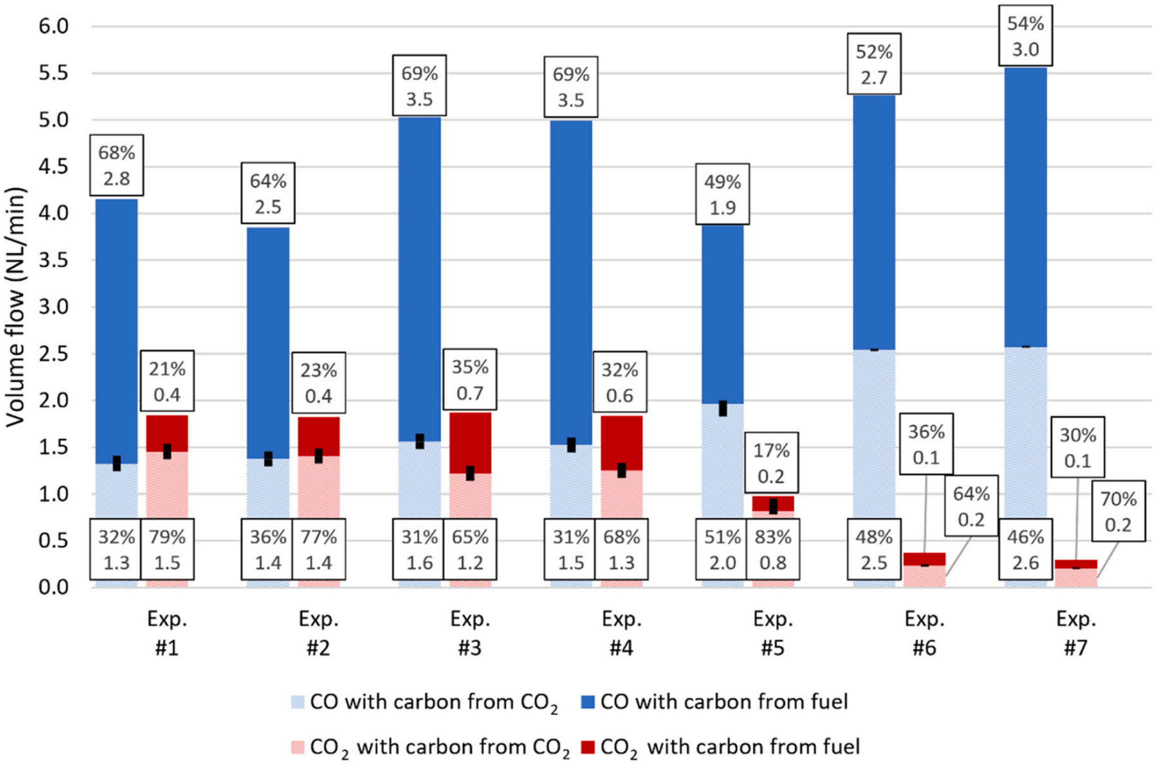

Fig. 5. Parental carbon sources of carbonaceous product gas components CO and CO_2. Percentage values refer to the relative contribution of carbon sources, expressed as $Y_{CO\ from\ CO2}$, $Y_{CO\ from\ fuel}$, $Y_{CO2\ from\ CO2}$, and $Y_{CO2\ from\ fuel}$.

carbon contribution of CO_2 to CO declining at higher fuel feeding rates is a significant effect.

3.2.3. Parental carbon sources of CO_2 in product gas

The total volume flow of CO_2 in product gas is similar for all softwood experiments (red bars in Fig. 5). Attributing carbon dioxide in the product gas to its parental carbon sources, fuel and CO_2, shows that higher fuel:CO_2 ratios decrease $Y_{CO2\ from\ CO2}$ by lowering the amount of CO_2 with carbon from CO_2 and increasing the amount of CO_2 with carbon from fuel. The decrease in CO_2 with carbon from CO_2 is explained by the increased conversion of CO_2 at higher fuel-gas contact times [15]. This effect is much more pronounced in experiments with wood char than softwood. This difference could be caused by the high levels of unconverted char that were calculated (Table 4) for experiments #6 and #7, which likely resulted in a significant increase in fuel-gas contact time compared to experiment #5. Similarly, in all softwood experiments the values of unconverted fuel carbon were lower and CO_2 with carbon from CO_2 was higher than in experiment #5. One conclusion from these data could be that for ideal CO_2 conversion, an excess of char should be kept in the gasification reactor to reach higher fuel-gas contact times.

For softwood as fuel, increased CO_2 with carbon from fuel can be explained by increased pyrolysis activity when more fuel is present. For experiments with wood char as a fuel, CO_2 with carbon from fuel is not increased at higher fuel feeding rates. Instead, slightly less CO_2 with carbon from fuel is observed in experiment #6 compared to #5. One explanation could be, that the CO_2 released from pyrolysis reacts with fuel to CO, same as for CO_2 fed as fuel. The increased fuel-gas contact time in experiments with higher wood char feeding rates might have increased the conversion more than the addition of pyrolytic CO_2, because of wood char's low volatile content. For high conversion of pyrolytic CO_2, one option for process improvement could be the adoption of in-bed feeding. Since in-bed feeding would move the point of CO_2 release away from the gas drain and towards the CO_2 inlet, thereby increasing fuel-gas contact time, the pyrolytic CO_2 might be converted to CO more efficiently.

3.2.4. Conversion of feedstock CO_2

While differences in CO_2 conversion were already indirectly used to explain observed carbon conversion trends in Sections 3.2.2 and 3.2.3, this chapter explicitly calculates X_{CO2} according to Eq. 24. It compares the results in Fig. 6 to the calculation by other methods described in Section 2.3.2. Error ranges are calculated based on the precision of EA-IRMS and GC-C-IRMS measurements without the hypothetical sampling error.

X_{CO2} is significantly higher when using char as feedstock than when using softwood. Temperature differences are ruled out as an explanation because the highest (903 °C) and lowest (821 °C) average temperatures in the reaction zone are measured during experiments with softwood as fuel (Table 3). One reason might be found in softwood's lower fixed carbon content and calculated unconverted char, suggesting that the bed height during these experiments might also have been lower, decreasing the fuel-gas contact time and lowering CO_2 conversion. This hypothesis is also supported by higher observed CO_2 conversions when more fuel is fed. This effect is especially pronounced for char as fuel, where more than 90% of feedstock CO_2 is converted. Another reason might be the difference in fuel characteristics. Surface area and porosity, active sites, mineral content, and particle size are suggested by comprehensive literature to affect char reactivity [5,8]. Char morphology is determined by reactive atmosphere, residence time, and temperature [8,48]. Higher pyrolysis temperatures are reported to reduce char reactivity [49]. This suggests that the higher temperatures for in-situ pyrolysis of softwood could lead to lower reactivity of the remaining char compared to the wood char previously prepared at 700 °C. Another reason might be the difference in mineral content between both fuels, which is regularly reported to catalyze gasification [5,8]. Related to their fixed carbon content, the softwood fuel has 1.37 wt%, while the wood char derived from Eucalyptus has 7.39% ash content. The higher amount of catalytically active ash elements in wood char, like Fe_2O_3, CaO, MgO, Na_2O,

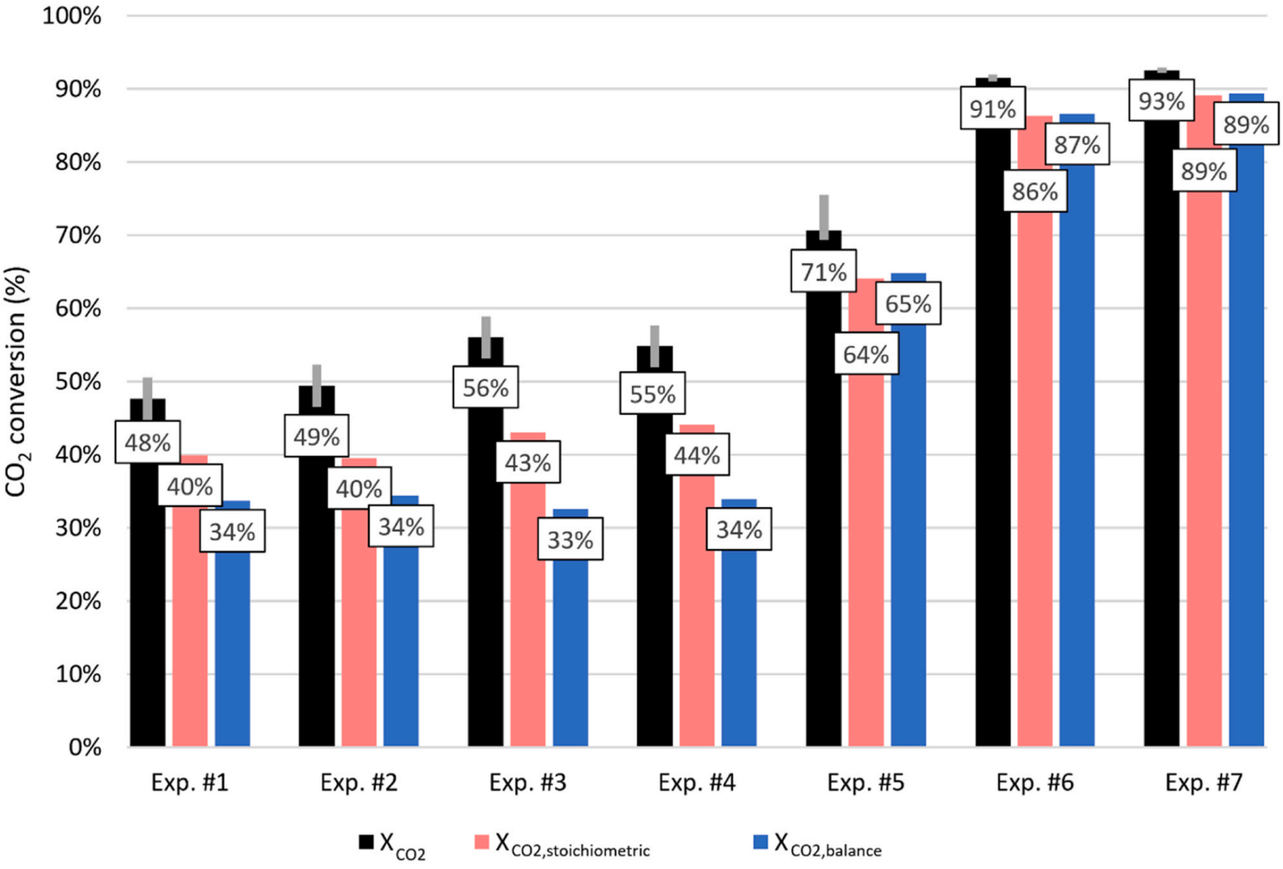

Fig. 6. Comparison of CO_2 conversion calculated by different methods.

and K_2O could have contributed to the observed increase in X_{CO2} upon using wood char as fuel.

Both simplified calculation results, $X_{CO2,stoichiometric}$ and $X_{CO2,balance}$ are lower than the X_{CO2} values, which are calculated based on stable carbon isotope analysis. The average gaps for $X_{CO2,stoichiometric}$ are 10% for using softwood as a fuel (Exp #1 - #4) compared to 5% for char (Exp #5 - #7). For $X_{CO2,balance}$, these numbers are 18% and 5% of average difference. This difference can be explained by the simplified calculation methods' inability to identify CO_2 produced from fuel; therefore, they underestimate how much feed CO_2 has been converted. Because of its higher volatile content, more CO_2 is produced from rapid devolatilization when using softwood, which leads to a sizeable error in determining the CO_2 conversion by mass balancing ($X_{CO2,balance}$). The differences in calculation results decrease when X_{CO2} approaches 100%, as all methods calculate the conversion as 100% if no CO_2 is present in the product gas. Therefore, a conclusion could also be that stable carbon isotope analysis significantly improves process understanding when CO_2 conversion is incomplete. These results prove why a reliable measurement method for these data is paramount.

4. Conclusion

The central part of this work is the application of stable carbon isotope analysis to measure the conversion of CO_2 in this system. A comparison with common calculation methods revealed that the new method yields CO_2 conversion results up to 23% points higher than calculated by mass balance. Other methods had considerable trouble identifying the CO_2 conversion when additional CO_2 was formed from the biomass by pyrolytic decomposition. The new method uses stable carbon isotope ratio analysis to differentiate between CO_2 formed from fuel and unconverted CO_2 fed as feedstock. This ability to differentiate can help to improve process understanding, facilitate technical development, and underpin biomass CO_2 gasification's position as carbon capture and utilization technology. The presented analysis did not use a dedicated tracing substance, which could potentially incur significant costs. When char was used as fuel, around 50% of carbon monoxide was produced from CO_2, proving that biomass CO_2 gasification can utilize CO_2 as a resource very effectively. The new method can also help to answer legislative questions around carbon accounting.

This work contains experimental data from seven continuous feeding gasification experiments in a fluidized bed reactor. The product gas from these experiments had reduction potentials up to 14, significantly higher than typical values for reducing gas in existing direct reduction ironmaking plants, which are reported around 9. From a reduction potential standpoint, these gases could be directly used for direct reduction ironmaking without intermediate gas reforming or separation steps. Further investigation should be dedicated to clarifying if any and which technological steps are needed for direct connection of these processes, e.g., a tar separation step or removing other impurities. Still, CO_2 biomass gasification should be considered for application in ironmaking. When hydrogen is added from an external source like water electrolysis to adjust the H_2-to-CO ratio, the CO-rich product gas could also be used as a feedstock for chemical synthesis.

A limitation of this study is that some assumptions were necessary for evaluation because of missing data, e.g., assuming the isotopic fractionation factor for CO_2 in the product gas as 0 based on the literature. Measuring the stable carbon isotope ratio for products other than CO and CO_2 would also allow the calculation of this factor and improve the results. If feedstocks with similar isotopic abundance are used, enriching or depleting feedstock CO_2 by adding $^{13}CO_2$ or $^{12}CO_2$ might be necessary to reduce the uncertainty. Additionally, this work only contains a small number of experiments and is focused on establishing stable carbon isotope analysis as a tool for carbon stream analysis in CO_2 biomass gasification. A more extensive experimental campaign using this new method to look more closely into the effects of water/CO_2 mixtures as feed, temperature, bed material variations, and other factors could improve process understanding further.

Nevertheless, these results provide critical insights into the CO_2 gasification process and can be used for further technical development. The sharp increase in CO_2 conversion when feeding more char as fuel confirms the importance of gas-solid contact time identified in previous works [15]. Based on this observation, a process improvement could be to optimize the contact time by leaving excess solid carbon in the gasification reactor, even if the system is operated as a circulating or bubbling fluidized bed. Another improvement could be to adjust the point of volatile release such that CO_2 released by rapid devolatilization of fuels is also in prolonged contact with the fuel bed. This adjustment could reduce CO_2 generated from biomass in product gas by increased conversion to CO. This effect could be achieved by in-bed feeding of fuel instead of on-bed feeding. Another possibility would be to have a dedicated pyrolysis step before gasification, which could also lower the CO_2 content in produced gases based on the data in this work.

CRediT authorship contribution statement

Franz Winter: Writing – review & editing, Supervision, Resources, Project administration, Funding acquisition, Conceptualization. **Stefan Müller:** Supervision, Resources, Project administration, Funding acquisition, Conceptualization. **Josef Fuchs:** Writing – review & editing, Supervision, Resources, Project administration, Funding acquisition, Data curation, Conceptualization. **Florian Johann Müller:** Writing – review & editing, Writing – original draft, Visualization, Validation, Software, Methodology, Investigation, Formal analysis, Data curation, Conceptualization.

Declaration of Competing Interest

The authors declare that they have no known competing financial interests or personal relationships that could have appeared to influence the work reported in this paper.

Data Availability

Data will be made available on request.

Acknowledgments

This study was carried out within the doctoral college *CO_2Refinery* at TU Wien. The authors would like to thank *Imprint Analytics GmbH* (Neutal, Austria) for measuring stable carbon isotope ratios and providing advice for the sampling procedure. The authors acknowledge *TU Wien Bibliothek* for financial support through its Open Access Funding Programme.

Appendix A. Fluidization calculations

General information on the equations and assumptions for calculating the fluidization state of particles was described in previous work; see Müller et al. Appendix A, which contains data for Olivine and wood char [15].

The softwood pellets have a diameter of 6 mm, which is assumed as the particle size d_p for softwood pellets. At an average length of 10 mm, the sphericity for softwood pellets is calculated as 0.85 using Eq A-1. 750 kg/m^3 are used for the density of wood pellets.

$$d_{sv} = \Phi^* d_P \tag{A-1}$$

The results of fluidization calculations summarized for Olivine, softwood pellets, and three size classes of wood char are given in Table A-1. Feed gas flow rates were selected at around 3 NL/min to form a bubbling fluidized bed from Olivine while keeping gas velocities low to increase fuel-gas contact time.

Table A-1
Fluidization properties of all used bed materials at 1200 K and atmospheric pressure [15].

		Olivine	Softwood pellets	Small char	Medium char	Large char
d_P	m	3.37E-04	6.00E-03	1.65E-03	3.75E-03	6.50E-03
Φ	-	7.60E-01[50]	8.50E-01	6.60E-01[51]	6.60E-01[51]	6.60E-01[51]
d_{SV}	m	2.56E-04	5.10E-03	1.09E-03	2.48E-03	4.29E-03
ρ_F (1200 K	kg/m^3	4.34E-01	4.34E-01	4.34E-01	4.34E-01	4.34E-01
ρ_P	kg/m^3	2.85E+03[52]	7.50E+02	1.70E+02[51]	1.70E+02[51]	1.70E+02[51]
μ (1200 K	N*s/m^2	4.68E-05[53]	4.68E-05	4.68E-05[53]	4.68E-05[53]	4.68E-05[53]
g	m/s^2	9.81E+00	1.08E+01	9.81E+00	9.81E+00	9.81E+00
Ar	-	9.32E+01	2.13E+05	4.26E+02	5.00E+03	2.60E+04
u_{mf}	m/s	2.37E-02	1.38E+00	2.54E-02	1.26E-01	3.31E-01
A	m^2	2.21E-03	2.21E-03	2.21E-03	2.21E-03	2.21E-03
$\dot{V}_{mf}$	Nm^3/h	4.31E-02	2.51E+00	4.62E-02	2.29E-01	6.02E-01
f_{umf} (2.8 NL/min)	-	3.90	0.07	3.64	0.73	0.28
f_{umf} (3.0 NL/min)	-	4.18	0.07	3.90	0.79	0.30
f_{umf} (3.2 NL/min)	-	4.45	0.08	4.16	0.84	0.32

Appendix B. Mass balancing in IPSEpro 8.0 in this work

General information on IPSEpro 8.0 and its use in gasification modeling is available in the literature, e.g., [54] and other publications by TUW. This work used a gasifier model typically used to simulate the gasification reactor of a dual-fluidized bed gasifier (Figure B-1)

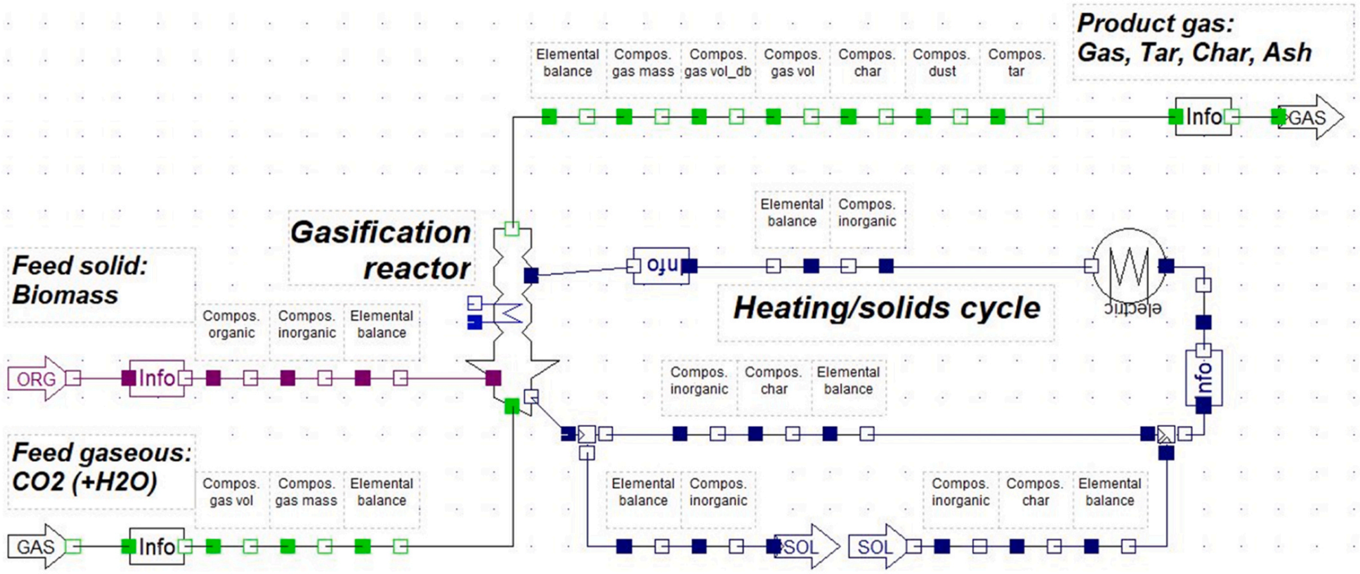

Figure B-1. Flowsheet model of gasifier used for mass balancing in IPSEpro 8.0.

The model has three inlets (fully colored connectors) and two outlets (empty connectors). Since IPSEpro is an equation-oriented tool, the number of equations must equal the number of variables. The model presented in Figure B-1 has nearly 1600 variables. Most input relevant to mass balancing is given as composition data. The biomass composition is known from proximate and ultimate analysis (Table 2). The feed gas composition is pure CO_2 or CO_2 mixed with water, as given in the experimental matrix (Table 3). Dry-based composition data of CO, CO_2, CH_4, H_2, and O_2 is available from continuous analysis. The average data from one hour of stable operation are used for the product gas composition. Ash and bed material are simplified to singular substances with unchanging composition. The inlet and outlet in the solids cycle are necessary for model convergence. Nothing other than Olivine and ash is drained or added to the system in this cycle. The heating/solids cycle's primary function in the model is to close the energy balance, which is not the focus of this paper.

The only absolute values in the mass balance are for the flow rates of the feeding lines. The volume flow rate of CO_2 fed to the reactor ($\dot{V}_{CO2,in}$), which was set using a rotameter and checked by a gas clock, is one of these two. The other absolute value is the biomass feed rate, set in the model relative to the gas inlet. The tar concentration in the product gas is assumed as 6.3 g/m$^3_{stp,db}$ as given by literature for using CO_2 to gasify softwood pellets in a fluidized bed with Olivine as bed material [55]. The elemental tar composition was assumed to match the tar composition measured by GC/MS in CO_2 gasification experiments with softwood pellets as fuel, e.g., [56], and is 92.8 wt% carbon, 7.0 wt% hydrogen, and 0.1 wt% oxygen. The share of fuel remaining in the reactor or entrained as ungasified char is not experimentally determined but can be calculated from the model. Ungasified char is assumed to match the elemental composition of wood char, which is used as fuel in this work (Table 2). Ungasified char is treated as an outgoing stream to allow for a steady state calculation in this black box model. With these data, the outgoing volume flows of CO ($\dot{V}_{CO,out}$) and CO_2

($\dot{V}_{CO2,out}$), which are needed for Eq. 23 - Eq. 24, can be derived from mass balancing. The global hydrogen balance allows for calculating the product gas's water content.

Stable carbon isotope ratios are used to build a ^{12}C balance as an additional equation (Eq. 19). This means that not only must the global mass balance for carbon yield the same input and output to the process, but more specifically, the exact requirement is asked of ^{12}C. When the global carbon balance and ^{12}C balance are fulfilled, so is the ^{13}C balance. The isotopic enrichment factor ε_{CO} and the mean isotope ratio of all carbonaceous outputs other than CO and CO_2 ($\delta^{13}C_{rest,out}$) are calculated from these isotopic and global mass balances. Two more boundary conditions, which come from assumptions, are necessary for these calculations. The first assumption is that ε_{CO2} is assumed zero, and the second is that CO_2 is only converted to CO (see Section 2.3 for more information). The so-calculated $\delta^{13}C_{rest,out}$ value is sensitive to error since minimal absolute changes lead to a sizeable deviation from zero in the VPDB scale (see Eq. 14). For this reason, it can be compared to the isotope ratio measurement of used biomass and used as a plausibility check for the whole balance.

Appendix C. Supporting information on experimental data

Experimental data are plotted in Figure C-1 for one experiment with each fuel type. Experiment #6 was conducted with wood char as fuel, while softwood pellets were used in experiment #3. The CO_2 conversion $X_{CO2,stoichiometric}$ is calculated using the simplified calculation as per Eq. 25. This equation estimates the CO_2 conversion at the same time interval of product gas composition data, which is every 1 s. Temperature measurements are positioned as given in Fig. 2. Stream composition data is adjusted to remove N_2, which was used for purging the pressure measurement and fuel tank. Without adjustment, this N_2 is under 5 vol% of the total gas stream going to the measurement. Both experiments were conducted with dry CO_2 feed, and the parental carbon ratio of fuel to feedstock CO_2 in both experiments was two.

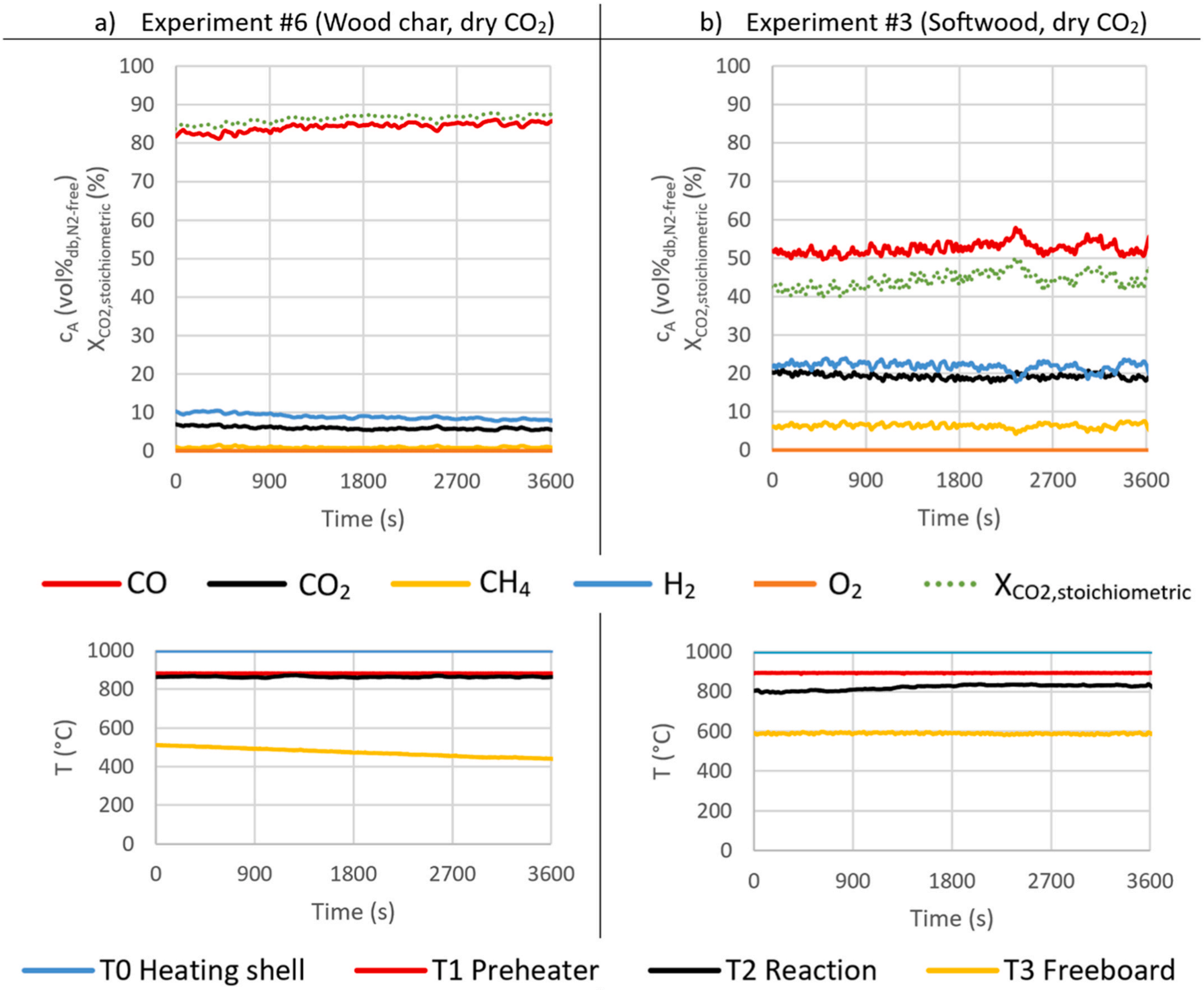

Figure C-1. Comparison of experimental data using different fuel types: a) wood char (left, experiment number #6), b) softwood pellets (right, experiment number #3). $X_{CO2,stoichiometric}$ is calculated by the simplified method given in Eq. 25.

The temperature *T0 Heating shell* in this reactor is limited to 1000 °C, equal for both experiments. *T2 Reaction* is the measurement at the center of the fuel-filled zone. The temperature here is around 40 °C lower during experiment #3 using softwood compared to #6 using wood char. *T3 Freeboard* measures the temperature of the gas phase above the fluidized bed but inside the reactor. Contrary to *T2 Reaction*, *T3 Freeboard* averages around 100–200 °C higher when softwood is used as fuel. These observations cannot be explained with certainty because of a lack of information on the power supplied by the heating shells, heat losses, and heat transmission phenomena in and around the reactor. Interpretations for both differences are suggested by the mass and energy balance conducted in IPSEpro. The difference in freeboard temperature could be due to a significant amount of fuel surplus not converted during experiment #6 with wood char. According to the mass balance, around 46% of carbon fed via wood char was not converted, significantly higher than the 12% calculated for experiment #3 feeding softwood. While some of this surplus was leaving the reactor as fly char, in experiment #6, this surplus likely slowly built up in the reactor towards the freeboard. Char accumulation at some point before or during the experiments was also noticeable from ongoing CO production after the main investigation period had ended and no new fuel was added. CO was still produced when only CO_2 was fed after each experiment (except experiment #6). Due to uncertainties in volume flow after the investigated period, no values are estimated for the total char at the experiments' end. An explanation for the declining freeboard temperature could be that the rising bed transmits more energy to ambient through the reactor walls because the reactor is not as well insulated above the heating shell. The difference in reaction zone temperature can be explained by an increased cooling effect from endothermic pyrolysis reactions. The fluctuations in product gas concentration are consistently higher for softwood pellets than for char. The reason for this is the instability induced by the somewhat discontinuous feeding of fuel particles by the screw feeder, which is delivering discrete fuel particles. The larger softwood particles lead to small spikes in gas measurement because of rapid devolatilization [8]. This effect is expected to be absent in larger plants with higher feeding rates.

The equipment used in this study has the following error tolerances:

- Dry gas composition measurement: 1 vol% of calibrated maximum. The calibrated maxima were
  - 100 vol% CO_2
  - 100 vol% CO
  - 10.1 vol% CH_4
  - 20.9 vol% O_2
  - 100 vol% H_2
- Temperature measurement by thermocouple type K: 4‰ of measured temperature
- EA-IRMS: ±0.63‰ with and ±0.3‰ without hypothetical sampling error
- GC-C-IRMS: ±1.10‰ with and ±0.5‰ without hypothetical sampling error
- The rotameter used for controlling the flow rate of CO_2 fed to the reactor has been compared to a gas clock with a precision of ±3‰ before experiments.

References

[1] IPCC, Climate Change, The Physical Science Basis. Contribution of Working Group I to the Sixth Assessment Report on the Intergovernmental Panel on Climate Change, Cambridge University Press, Cambridge, 2021, p. 2021, https://doi.org/10.1017/9781009157896.

[2] IPCC, Climate Change, Mitigation of Climate Change. Contribution of Working Group III to the Sixth Assessment Report of the Intergovernmental Panel on Climate Change, Cambridge University Press, Cambridge, 2022, p. 2022, https://doi.org/10.1017/9781009157926.

[3] IRENA and Methanol Institute, Innovation Outlook: Renewable Methanol, Abu Dhabi, 2021.

[4] S. De, A.K. Agarwal, V.S. Moholkar, B. Thallada. Coal and Biomass Gasification, 1st ed., Springer, Singapore, 2018. ⟨https://doi.org/10.1007/978-981-10-7335-9⟩.

[5] Y.H.Chan, S.N.F. Syed Abdul Rahman, H.M.Lahuri, A.Khalid, Recent progress on CO-rich syngas production via CO2 gasification of various wastes: A critical review on efficiency, challenges and outlookEnviron. Pollut.278202111610.1016/j. envpol.2021.116843.

[6] A. Nurdiawati, I.N. Zaini, W. Wei, R. Gyllenram, W. Yang, P. Samuelsson, Towards fossil-free steel: Life cycle assessment of biosyngas-based direct reduced iron (DRI) production process, J. Clean. Prod. 393 (2023) 136262, https://doi.org/10.1016/j.jclepro.2023.136262.

[7] A. Bhagavatula, G. Huffman, N. Shah, C. Romanek, R. Honaker, Source apportionment of carbon during gasification of coal-biomass blends using stable carbon isotope analysis, Fuel Process. Technol. 128 (2014) 83–93, https://doi.org/10.1016/j.fuproc.2014.06.024.

[8] P. Lahijani, Z.A. Zainal, M. Mohammadi, A.R. Mohamed, Conversion of the greenhouse gas CO2 to the fuel gas CO via the Boudouard reaction: A review, Renew. Sustain. Energy Rev. 41 (2015) 615–632, https://doi.org/10.1016/j.rser.2014.08.034.

[9] S. Müller, Hydrogen from biomass for industry - industrial application of hydrogen production based on dual fluid gasification, Dissertation, Technische Universität Wien, 2013. ⟨https://resolver.obvsg.at/urn:nbn:at:at-ubtuw:1-96540⟩.

[10] M. Pohořelý, M. Jeremiáš, K. Svoboda, P. Kameníková, S. Skoblia, Z. Beňo, CO2 as moderator for biomass gasification, Fuel 117 (2014) 198–205, https://doi.org/10.1016/j.fuel.2013.09.068.

[11] X. Yao, Q. Yu, Z. Han, H. Xie, W. Duan, Q. Qin, Kinetics of CO2 gasification of biomass char in granulated blast furnace slag, Int J. Hydrog. Energy 43 (2018) 12002–12012, https://doi.org/10.1016/j.ijhydene.2018.04.102.

[12] N. Sadhwani, S. Adhikari, M.R. Eden, Biomass Gasification Using Carbon Dioxide: Effect of Temperature, CO2/C Ratio, and the Study of Reactions Influencing the Process, Ind. Eng. Chem. Res 55 (2016) 2883–2891, https://doi.org/10.1021/acs.iecr.5b04000.

[13] Z. Wang, X. Liu, K.G. Burra, J. Li, M. Zhang, T. Lei, A.K. Gupta, Towards enhanced catalytic reactivity in CO2-assisted gasification of polypropylene, Fuel 284 (2021) 1–9, https://doi.org/10.1016/j.fuel.2020.119076.

[14] P. Lahijani, M. Mohammadi, Z.A. Zainal, A.R. Mohamed, Advances in CO2 gasification reactivity of biomass char through utilization of radio frequency irradiation, Energy 93 (2015) 976–983, https://doi.org/10.1016/j.energy.2015.09.092.

[15] F.J. Müller, J. Fuchs, M. Fanjul, A.O. Guti, S. Pratschner, S. Müller, F. Winter, CO2 conversion to CO by fluidized bed biomass gasification: Analysis of operational parameters, J. CO2 Util. 81 (2024), https://doi.org/10.1016/j.jcou.2024.102706.

[16] M. Jeremiáš, M. Pohořelý, K. Svoboda, V. Manovic, E.J. Anthony, S. Skoblia, Z. Beňo, M. Šyc, Gasification of biomass with CO2 and H2O mixtures in a catalytic fluidised bed, Fuel 210 (2017) 605–610, https://doi.org/10.1016/j.fuel.2017.09.006.

[17] S. Valin, L. Bedel, J. Guillaudeau, S. Thiery, S. Ravel, CO2 as a substitute of steam or inert transport gas in a fluidised bed for biomass gasification, Fuel 177 (2016) 288–295, https://doi.org/10.1016/j.fuel.2016.03.020.

[18] S. Tong, L. Li, L. Duan, C. Zhao, E.J. Anthony, A kinetic study on lignite char gasification with CO2 and H2O in a fluidized bed reactor, Appl. Therm. Eng. 147 (2019) 602–609, https://doi.org/10.1016/j.applthermaleng.2018.10.113.

[19] C. Liang, H. Zhang, Z. Zhu, Y. Na, Q. Lu, CO2-O2 gasification of a bituminous coal in circulating fluidized bed, Fuel 200 (2017) 81–88, https://doi.org/10.1016/j.fuel.2017.03.032.

[20] K. Liu, Z. Yuan, C. Shi, H. Zhao, H. Wang, Effect of CaO-SiO2-FeO slag system on coal gasification reaction in CO2-Ar atmosphere and kinetic analysis, J. CO2 Util. 56 (2022) 101850, https://doi.org/10.1016/j.jcou.2021.101850.

[21] A. Lampropoulos, N. Kaklidis, C. Athanasiou, M.A. Montes-Morán, A. Arenillas, J. A. Menéndez, V.D. Binas, M. Konsolakis, G.E. Marnellos, Effect of Olive Kernel thermal treatment (torrefaction vs. slow pyrolysis) on the physicochemical characteristics and the CO2 or H2O gasification performance of as-prepared biochars, Int J. Hydrog. Energy 46 (2021) 29126–29141, https://doi.org/10.1016/j.ijhydene.2020.11.230.

[22] L. Reyes, L. Abdelouahed, B. Campusano, J.C. Buvat, B. Taouk, Exergetic study of beech wood gasification in fluidized bed reactor using CO2 or steam as gasification agents, Fuel Process. Technol. 213 (2021) 1–12, https://doi.org/10.1016/j.fuproc.2020.106664.

[23] N. Spiegl, X. Long, C. Berrueco, N. Paterson, M. Millan, Oxy-fuel co-gasification of coal and biomass for negative CO2 emissions, Fuel 306 (2021) 1–8, https://doi.org/10.1016/j.fuel.2021.121671.

[24] R. Liu, Y. Zhang, Z. Ling, Y. Song, Some new insights into the synergy occurring during char gasification in CO2/H2O mixtures, Fuel 268 (2020) 1–8, https://doi.org/10.1016/j.fuel.2020.117307.

[25] Z. Liu, F. Zhang, H. Liu, F. Ba, S. Yan, J. Hu, Pyrolysis/gasification of pine sawdust biomass briquettes under carbon dioxide atmosphere: Study on carbon dioxide reduction (utilization) and biochar briquettes physicochemical properties, Bioresour. Technol. 249 (2018) 983–991, https://doi.org/10.1016/j.biortech.2017.11.012.

[26] A.M. Mauerhofer, S. Müller, A. Bartik, F. Benedikt, J. Fuchs, M. Hammerschmid, H. Hofbauer, Conversion of CO2 during the DFB biomass gasification process, Biomass-.-. Convers. Biorefin 11 (2021) 15–27, https://doi.org/10.1007/s13399-020-00822-x.

[27] R. Liu, R. Tsiava, S. Xu, D. Chen, Experimental study of char gasification characteristics with high temperature flue gas, J. Energy Inst. 97 (2021) 187–193, https://doi.org/10.1016/j.joei.2021.04.015.

[28] Y. Cheng, Z. Thow, C.H. Wang, Biomass gasification with CO2 in a fluidized bed, Powder Technol. 296 (2016) 87–101, https://doi.org/10.1016/j.powtec.2014.12.041.

[29] European Commission, Directive (EU) 2023/2413 of the European Parliament and of the Council of 18 October 2023 amending Directive (EU) 2018/2001, Regulation (EU) 2018/1999 and Directive 98/70/EC as regards the promotion of energy from renewable sources, Official Journal of the European Union 2413 (2023) 1–77. ⟨https://eur-lex.europa.eu/legal-content/EN/TXT/?uri=CELEX%3A32023L2413&qid=1699364355105⟩.

[30] D. Leckel, Diesel production in coal-based high-temperature Fischer-Tropsch plants using fixed bed dry bottom gasification technology, Fuel Process. Technol. 92 (2011) 959–969, https://doi.org/10.1016/j.fuproc.2010.12.017.

[31] N.A. Matwiyoff, D.G. Ott, Stable isotope tracers in the life sciences and medicine, Science 181 (1979) (1973) 1125–1133, https://doi.org/10.1126/science.181.4105.1125.

[32] L.Z. Gannes, C.M. Del Rio, P. Koch, Natural Abundance Variations in Stable Isotopes and their Potential Uses in Animal Physiological Ecology, Comp. Biochem Physiol. A Mol. Integr. Physiol. 119 (1998) 725–737, https://doi.org/10.1016/S1095-6433(98)01016-2.

[33] I.S. Al-Aasm, B.E. Taylor, B. South, Stable isotope analysis of multiple carbonate samples using selective acid extraction, Chem. Geol.: Isot. Geosci. Sect. 80 (1990) 119–125, https://doi.org/10.1016/0168-9622(90)90020-D.

[34] F. Kapteijn, R. Meijer, J.A. Moulijn, D. Cazorla-Amóros, On why do different carbons show different gasification rates: A transient isotopic CO2 gasification study, Carbon N. Y 32 (1994) 1223–1231, https://doi.org/10.1016/0008-6223(94)90106-6.

[35] D. Cazorla-Amorós, A. Linares-Solano, C.S.M. de Lecea, F. Kapteijn, Assessment of the CO2-carbon gasification catalyzed by calcium. A transient isotopic study, Carbon N. Y 32 (1994) 423–430, https://doi.org/10.1016/0008-6223(94)90162-7.

[36] S. Flude, G. Johnson, S.M.V. Gilfillan, R.S. Haszeldine, Inherent Tracers for Carbon Capture and Storage in Sedimentary Formations: Composition and Applications, Environ. Sci. Technol. 50 (2016) 7939–7955, https://doi.org/10.1021/acs.est.6b01548.

[37] D.W. Hoffman, C. Rasmussen, Absolute Carbon Stable Isotope Ratio in the Vienna Peedee Belemnite Isotope Reference Determined by ^{1}H NMR Spectroscopy, Anal. Chem. 94 (2022) 5240–5247, https://doi.org/10.1021/acs.analchem.1c04565.

[38] W.A. Brand, T.B. Coplen, J. Vogl, M. Rosner, T. Prohaska, Assessment of international reference materials for isotope-ratio analysis (IUPAC technical report), Pure Appl. Chem. 86 (2014) 425–467, https://doi.org/10.1515/pac-2013-1023.

[39] IUPAC Commission on Atomic Weights and Isotopic Abundances, Atomic weights of the elements 1991, J. Phys. Chem. Ref. Data 22 (1993) 1571–1584. ⟨https://doi.org/10.1063/1.555933⟩.

[40] A.M. Mauerhofer, S. Müller, F. Benedikt, J. Fuchs, A. Bartik, H. Hofbauer, CO2 gasification of biogenic fuels in a dual fluidized bed reactor system, Biomass-.-. Convers. Biorefin 11 (2021) 1101–1116, https://doi.org/10.1007/s13399-019-00493-3.

[41] T. Pröll, H. Hofbauer, Development and application of a simulation tool for biomass gasification based processes, Int. J. Chem. React. Eng. 6 (2008), https://doi.org/10.2202/1542-6580.1769.

[42] Y. Bottinga, Calculated fractionation factors for carbon and hydrogen isotope exchange in the system calcite-carbon dioxide-graphite-methane-hydrogen-water vapor, Geochim Cosmochim. Acta 33 (1969) 49–64, https://doi.org/10.1016/0016-7037(69)90092-1.

[43] P. Richet, Y. Bottinga, M. Javoy, A Review of Hydrogen, Carbon, Nitrogen, Oxygen, Sulphur, and Chlorine Stable Isotope Fractionation Among Gaseous Molecules, Annu Rev. Earth Planet Sci. 5 (1977) 65–110, https://doi.org/10.1146/annurev.ea.05.050177.000433.

[44] R. Liu, R. Tsiava, S. Xu, D. Chen, Experimental study of char gasification characteristics with high temperature flue gas, J. Energy Inst. 97 (2021) 187–193, https://doi.org/10.1016/j.joei.2021.04.015.

[45] S. Pratschner, M. Hammerschmid, S. Müller, F. Winter, Evaluation of CO2 sources for Power-to-Liquid plants producing Fischer-Tropsch products, J. CO2 Util. 72 (2023) 102508, https://doi.org/10.1016/j.jcou.2023.102508.

[46] J. Solar, I. de Marco, B.M. Caballero, A. Lopez-Urionabarrenechea, N. Rodriguez, I. Agirre, A. Adrados, Influence of temperature and residence time in the pyrolysis of woody biomass waste in a continuous screw reactor, Biomass-.-. Bioenergy 95 (2016) 416–423, https://doi.org/10.1016/j.biombioe.2016.07.004.

[47] A.J. Fleisher, H. Yi, A. Srivastava, O.L. Polyansky, N.F. Zobov, J.T. Hodges, Absolute 13C/12C isotope amount ratio for Vienna PeeDee Belemnite from infrared absorption spectroscopy, Nat. Phys. 17 (2021) 889–893, https://doi.org/10.1038/s41567-021-01226-y.

[48] H.C. Butterman, M.J. Castaldi, CO2 as a carbon neutral fuel source via enhanced biomass gasification, Environ. Sci. Technol. 43 (2009) 9030–9037, https://doi.org/10.1021/es901509n.

[49] F. Min, M. Zhang, Y. Zhang, Y. Cao, W.P. Pan, An experimental investigation into the gasification reactivity and structure of agricultural waste chars, J. Anal. Appl. Pyrolysis 92 (2011) 250–257, https://doi.org/10.1016/j.jaap.2011.06.005.

[50] D. Kunii, O. Levenspiel. Fluidization engineering, 2nd ed., Butterworth-Heinemann, Bosten, London, singapore, Sydney, Toronto, Wellington, 1991. ⟨https://doi.org/10.1016/C2009-0-24190-0⟩.

[51] F. Scala, R. Chirone, P. Salatino, Combustion and attrition of biomass chars in a fluidized bed, Energy Fuels 20 (2006) 91–102, https://doi.org/10.1021/ef050102g.

[52] A.M. Mauerhofer, J.C. Schmid, F. Benedikt, J. Fuchs, S. Müller, H. Hofbauer, Dual fluidized bed steam gasification: Change of product gas quality along the reactor height, Energy 173 (2019) 1256–1272, https://doi.org/10.1016/j.energy.2019.02.025.

[53] A. Fenghour, W.A. Wakeham, V. Vesovic, The viscosity of carbon dioxide, J. Phys. Chem. Ref. Data 27 (1998) 31–39, https://doi.org/10.1063/1.556013.

[54] T. Pröll, H. Hofbauer, Development and application of a simulation tool for biomass gasification based processes, Int. J. Chem. React. Eng. 6 (2008), https://doi.org/10.2202/1542-6580.1769.

[55] A.M. Mauerhofer, F. Benedikt, J.C. Schmid, J. Fuchs, S. Müller, H. Hofbauer, Influence of different bed material mixtures on dual fluidized bed steam gasification, Energy 157 (2018) 957–968, https://doi.org/10.1016/j.energy.2018.05.158.

[56] A.M. Mauerhofer, J. Fuchs, S. Müller, F. Benedikt, J.C. Schmid, H. Hofbauer, CO2 gasification in a dual fluidized bed reactor system: impact on the product gas composition, Fuel 253 (2019) 1605–1616, https://doi.org/10.1016/j.fuel.2019.04.168.